Journal of Solid State Chemistry 184 (2011) 893–898

Contents lists available at ScienceDirect

Journal of Solid State Chemistry

journal homepage: www.elsevier.com/locate/jssc

Structurally-driven metal–insulator transition in $Ca_2Ru_{1-x}Cr_xO_4$ ($0 \le x < 0.14$): A single crystal X-ray diffraction study

T.F. Qi [a,b,*], M. Ge [a,c], O.B. Korneta [a,b], S. Parkin [a,d], L.E. De Long [a,b], G. Cao [a,b]

[a] Center for Advanced Materials, University of Kentucky, Lexington, KY 40506, USA
[b] Department of Physics and Astronomy, University of Kentucky, Lexington, KY 40506, USA
[c] High Magnetic Field Laboratory, University of Science and Technology of China, Hefei, Anhui 230026, PR China
[d] Department of Chemistry, University of Kentucky, Lexington, KY 40506, USA

ARTICLE INFO

Article history:
Received 12 November 2010
Received in revised form
5 February 2011
Accepted 20 February 2011
Available online 1 March 2011

Keywords:
Single crystal X-ray diffraction
Structurally-driven
Metal–insulator transition
Structure distortion

ABSTRACT

Correlation between structure and transport properties are investigated in high-quality single-crystals of $Ca_2Ru_{1-x}Cr_xO_4$ with $0 < x < 0.14$ using single crystal X-ray diffraction and by electronic studies. The parent compound was known to exhibit an intriguing first-order structurally driven metal–insulator (MI) transition at 357 K. Upon chromium doping on the ruthenium site, the metal–insulator transition temperature (T_{MI}) was drastically reduced, and is related to the competition between structural changes that occur upon Cr doping and with decreasing temperature. A strong suppression of structural distortions with increasing Cr substitution was identified. No clear T_{MI} can be observed when $x > 13.5\%$ and the system behaves as an insulator. Such a large, sharp metal–insulator transition and tuneable transition temperature may have potential applications in electronic devices.

1. Introduction

As the $n=1$ (single layer) member of the alkaline earth-ruthenium Ruddlesden-Popper series, $A_{n+1}Ru_nO_{3n+1}$ (A=Ca, Sr, etc.; $n=1-\infty$), Ca_2RuO_4 is isostructural with K_2NiF_4 at room temperature with the lattice constants $a=b=3.8163$ Å and $c=12.0250$ Å [1,2]. It undergoes an important phase transition involving octahedral tilting and cooperative Jahn–Teller distortions [2,3], which lead to a structurally driven insulator to "near" metal transition at 357 K [4]. Most remarkably, the resistivity in the basal plane changes by an astonishing ten orders of magnitude, from 10^9 Ω cm at $T=70$ K to 10^{-1} Ω cm at $T=580$ K [1]. The transition is so significant because Ca_2RuO_4 is on the interface between metal and insulator. The competition between bandwidth W and interaction U of d-orbitals and nearest-neighbor oxygen orbitals makes a highly sensitive balance of U/W ratio across the metal–nonmetal boundary, which can readily be tipped by small perturbations, with resultant pronounced changes in physical properties [2,5,6]. Since the metal–insulator transition is driven by structure changes [2,6,7], single crystal structural analysis should provide important insight into this system. However, to date, few structural studies have been reported in the literature [8–10]. Braden et al. [8]described a series of rotations of the RuO_6 octahedra around the long axis, combined with a tilt around an axis lying in the RuO_2 plane and their relation with magnetic properties and the metal–insulator transition. Friedt et al. [9] studied the effect of Sr doping on Ca site. Steffens et al. [10] studied the crystal and magnetic structures of Ca_2RuO_4 under different pressures and determined the structure change under high pressure in Ca_2RuO_4.

This work is the first case of Cr doping to Ca_2RuO_4. We chose controlled substitution of the quadrivalent Ru by trivalent or quadrivalent Cr in $Ca_2Ru_{1-x}Cr_xO_4$ because Cr substitution is uniquely effective for widening the stability range of the antiferromagnetic-metal state while preserving other properties [11]. By substituting elements with a different ionic radius and the same valence, bandwidth can be controlled relative to the amplitude of the local electron–electron interaction by keeping the electron density fixed at a commensurate value [12]. This approach is advantageous to the study of lattice structure, especially the distortion of RuO_6 octahedra, and its direct relation with transport properties. In this work we report the synthesis and structure analyses based on single-crystal X-ray diffraction of the Cr doped compound $Ca_2Ru_{1-x}Cr_xO_4$, including crystal structure distortions and the associated changes in transport properties.

2. Experimental details

Large single crystals of $Ca_2Ru_{1-x}Cr_xO_4$ were grown by the Floating Zone method. A feed rod was made from powders of $CaCO_3$(Alfa Aesar, 99.99%), RuO_2(Colonial Metals, 99.99%) and

* Corresponding author at: 177 Chemistry-Physics Building University of Kentucky, Lexington, KY 40506-0055, USA
E-mail address: tqi2@uky.edu (T.F. Qi).

0022-4596/$ - see front matter © 2011 Elsevier Inc. All rights reserved.
doi:10.1016/j.jssc.2011.02.020

Cr_2O_3(Alfa Aesar, 99.99%) in calculated stoichiometric amounts. These were thoroughly mixed and reacted in air at 1050 °C for 24 h. The pre-heated powder was formed into a cylindrical shape 7–9 mm in diameter and 90–110 mm in length, and then pressed at a hydrostatic pressure of 300 MPa. The rods were sintered at 1200 °C for 24 h in air. The heating and cooling rates were 100 °C/h. Higher rate may lead to crushing of the rods after cutting and mounting in air. The equipment used for crystal growth was a 2-mirror type image furnace equipped with two 1000 W halogen lamps as heat source. The growth conditions were as follows: the seed and feed shafts were rotated in opposite directions at rates of 10–15 rpm; the shaft travel rate was 10 mm/h. Oxygen pressures of 0.2 bar were applied during the growth.

The Cr concentration was determined by Energy Dispersion X-ray (EDX) analysis, and results of X-ray diffraction and EDX indicated that all crystals studied were single phase. Resistivity was measured by a standard four-probe method with a superconducting quantum interference device (SQUID) from Quantum Design on bulk single crystal samples. All measurements of structure and resistivity were performed on same sample for each Cr concentration to ensure the reproducibility, though single-crystal diffraction required small pieces to be cut from the whole. The structures at different temperatures and different concentrations were examined on a Nonius–Kappa CCD X-ray single-crystal diffractometer and refined using SHELX programs [13]. All structures were strongly affected by absorption and extinction. All data were corrected for anisotropic absorption by comparison of symmetry equivalent reflections using the program SADABS [14]. Extinction proved to be more of a challenge. The extinction-correction facility within SHELXL [13] provides a purely isotropic treatment, but it was clear that extinction was severely anisotropic, and in the most severe cases, prevented stable structure refinement. The empirical program XABS2 [15], has been observed to correct for extinction effects [16]. In conjunction with the isotropic correction available in SHELXL, this gave a dramatic, albeit approximate, treatment of anisotropic extinction that was sufficient to allow stable refinement. 3-D structure drawings were created using DIAMOND [17]. Atomic positions, displacement parameters, and oxygen site occupancies were allowed to refine independently. All structures for $Ca_2Ru_{1-x}Cr_xO_4$ determined here with $x=0$, 0.032, 0.067, 0.092 and 0.135 at both 90 and 295 K had the symmetry of space group *Pbca*, and all feature a rotation of the RuO_6 octahedral about the *c*-axis with a tilt about an axis parallel to an edge of the octahedron basal plane.

3. Results and discussion

3.1. Room temperature structure of $Ca_2Ru_{1-x}Cr_xO_4$

$Ca_2Ru_{1-x}Cr_xO_4$ consists of layers of RuO_6 octahedrons with Ca between the layers (Fig. 1a). Note that the neighboring layers are not stacked exactly on top of each other, but are offset with respect to each other. This pattern clearly demonstrates the enormous structural distortion in this system. The in-plane tilt and rotation around the *c* axis of RuO_6 octahedra is readily apparent and all the distortion angles can be measured directly. The neighboring octahedra tilt in an ordered way, which becomes clearer in a projection of the unit cell on the *ac* plane (Fig. 1b). The layers are formed by corner-sharing RuO_6 octahedra. Looking down on the *ab* plane, we find that octahedra on the same layer rotate left and right alternately along the [1 1 0] direction (Fig. 1c). That reflects the change of Ru–O–Ru bond angle, which should be 180° in the ideal case.

$Ca_2Ru_{1-x}Cr_xO_4$ has only one Ru position, so Cr is doped on that site. The room-temperature lattice parameters (Table 1) agree well

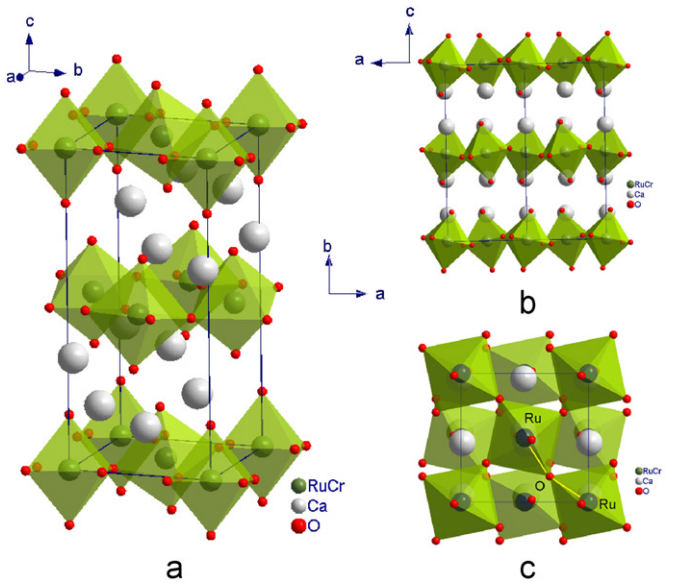

Fig. 1. Room-temperature structure of $Ca_2Ru_{1-x}Cr_xO_4$. (a) Structure at 290 K; (b) projection onto the *ac* plane; and (c) projection onto the *ab* plane.

with literature values [1,8] and theoretical values [18]. An important feature of this structure is that there is only one in-plane oxygen position, which means all in-plane oxygen ions have the same distance to the planes formed by the Ru atoms.

3.2. Temperature dependence of the $Ca_2Ru_{1-x}Cr_xO_4$ structure

The cell parameters all changed significantly with decreasing temperature. These changes were not simply a result of thermal contraction because they were not uniform. Indeed, we observed opposite trends for cell parameters parallel and perpendicular to the direction of buckling of the layers. Comparing high temperature and low temperature lattice parameters in Fig. 2, it is clear that *a* and *b* are elongated while *c* shrink, reflecting the flattening of RuO_6 octahedra, which is expected to greatly influence the crystal field that determines electron occupancy in the triply degenerate orbital state of ruthenate. It was ascertained to arise from a Jahn–Teller effect [8]. The temperature dependence of the lattice constants and the volume in Fig. 2 is indicative of profound structural changes. Moreover, the lattice volume *V* of $Ca_2Ru_{1-x}Cr_xO_4$ ($0<x<0.12$) abruptly *expands with cooling below* T_{MI}, giving rise to a total volume expansion $\Delta V/V\sim -0.9\%$ over the temperature range $90<T\leq 290$ K [2]. The orthorhombic distortion and the extremely large and anisotropic thermal expansions indicate a dominant structural distortion, which is frequently due to a rotation of the octahedral [8]. In $Ca_2Ru_{1-x}Cr_xO_4$ the RuO_6 octahedra have the freedom to rotate around an axis parallel to *c*, which is in turn related to the observed decrease of *b*.

Fig. 3 shows the temperature dependence of the three angles used to describe the tilt and distortion of the octahedra. We use the same definition as Braden et al. [8]: O1 is the oxygen on basal plane and O2 on top and bottom vertex. $\Theta-O1$ is the tilt angle between the octahedron basal plane and the *ab* plane. $\Theta-O2$ is the angle between the Ru–O2 bond and the *c* axis. Ru–O–Ru is the bond angle between two connected Ru–O bonds. Dramatic changes of all three distortion angles can be observed in Fig. 3. All the RuO_6 octahedra alternately rotate in opposite directions in the direction of infinite chains of corner-sharing RuO_6 octahedra. The big decrease of Ru–O–Ru bond angle and the big increase of both $\Theta-O1$ and $\Theta-O2$ on cooling show the incremental structure distortions with decreasing temperature. The Ru–O–Ru bond

Table 1
Experimental and refinement details of $Ca_2Ru_{1-x}Cr_xO_4$(x=0.067) at selected temperatures.

	90 K	190 K	290 K
Crystal data			
Chemical formula	$Ca_4Cr_{0.134}Ru_{1.866}O_8$	$Ca_4Cr_{0.134}Ru_{1.866}O_8$	$Ca_4Cr_{0.134}Ru_{1.866}O_8$
M_r	474.02	474.02	474.02
Crystal system, space group	Orthorhombic, *Pbca*	Orthorhombic, *Pbca*	Orthorhombic, *Pbca*
Temperature (K)	90	190	290
a, b, c (Å)	5.3917 (2), 5.5157 (2), 11.8804 (4)	5.3920 (3), 5.4432 (3), 12.0037 (6)	5.3359 (3), 5.3528 (3), 12.2571 (7)
V (Å^3)	353.31 (2)	352.31 (3)	350.09 (3)
Z	2	2	2
Radiation type	Mo $K\alpha$	Mo $K\alpha$	Mo $K\alpha$
μ (mm^{-1})	6.99	7.01	7.05
Crystal size (mm)	0.05 × 0.05 × 0.05	0.01 × 0.05 × 0.05	0.01 × 0.05 × 0.05
Data collection			
Diffractometer	Nonius KappaCCD diffractometer	Nonius KappaCCD diffractometer	Nonius KappaCCD diffractometer
Absorption correction	Multi-scan SADABS[a]	Multi-scan SADABS[a]	Multi-scan SADABS[a]
No. of measured, independent and observed[$I>2\sigma(I)$] reflections	7241, 398, 352	7265, 396, 260	7243, 403, 228
R_{int}	0.03	0.026	0.027
Refinement			
R[$F^2>2\sigma(F^2)$], $wR(F^2)$, S	0.016, 0.046, 1.13	0.028, 0.080, 1.10	0.016, 0.044, 1.14
No. of reflections	398	396	393
No. of parameters	36	36	36
No. of restraints	0	0	0
$\Delta\rho_{max}$, $\Delta\rho_{min}$ (e Å^{-3})	0.66, −0.60	1.33, −0.96	0.58, −0.57

[a] Ref. [14]

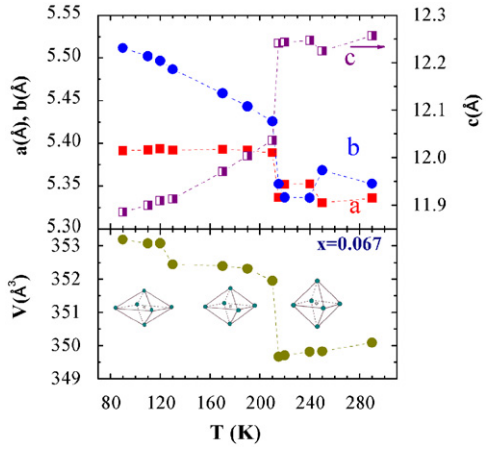

Fig. 2. Temperature dependence of the lattice parameters of $Ca_2Ru_{1-x}Cr_xO_4$(x=0.067), obtained from single-crystal X-ray diffraction. *Note*: In this and the following figures the scales for a, b are on left side and c on right side.

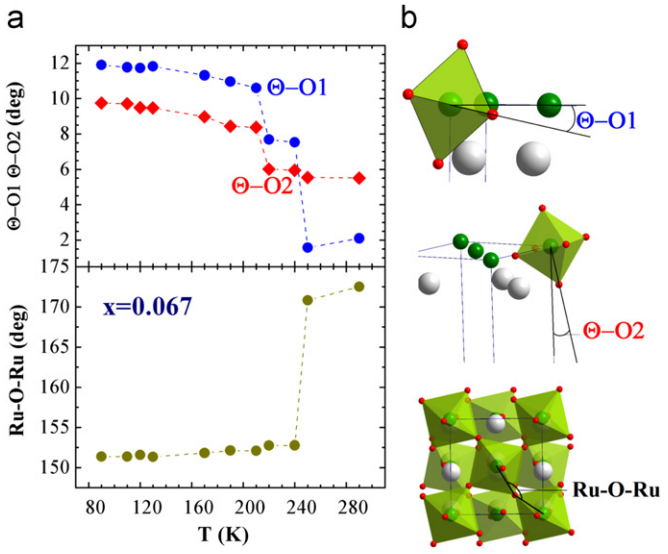

Fig. 3. (a) Temperature dependence of the tilt, rotation and bond angles in $Ca_2Ru_{1-x}Cr_xO_4$ (x=0.067), obtained from single-crystal X-ray diffraction; and (b) definition of $\Theta-O1$, $\Theta-O2$ and Ru–O–Ru distortion angles.

angle is considerably less than the ideal 180° and the decrease of Ru–O–Ru bond angle upon cooling shows the rotation of octahedra around the c axis. This implies insulating behavior due to narrowing of the d-electron bandwidth [1]. The temperature change provides sufficient perturbation to the system to tip the balance of U/W ratio across the metal–nonmetal boundary, resulting in an insulator.

3.3. *Cr concentration dependence of the $Ca_2Ru_{1-x}Cr_xO_4$ structure*

Another perturbation that can tip the balance of U/W ratio is impurity doping. The experimental and refinement details of the single crystal X-ray diffraction data are given in Table 2. The results of the full structure refinements and comparisons of bond lengths and distortion angles are given in Table 3. The Cr concentration dependence of the lattice constants was determined up to 13.5% (Table 3). The position of Ru atom is always (0,0,0). Ru–O–Ru means the bond angle between connected Ru–O bonds and the tilt angles are determined at the two oxygen sites. Note that the tilt is always around the b axis.

Selected Ru–O distances of $Ca_2Ru_{1-x}Cr_xO_4$ obtained at 90 K are also gathered in Table 3. O1 denotes the oxygen in the RuO_4 basal plane and O2 means the oxygen on top and bottom apex of an octahedron. The increase of Ru–O2 bond with increasing Cr doping is counter to the usual thermal expansion. The shrink of the in-plane bond is also remarkable. The overall elongation of the RuO_6 octahedra along the c axis might be associated with a Jahn–Teller distortion. Similar distortions of octahedra and large octahedral tilt angles are also reported in manganites [19] and vanadates [20,21].

Table 2
Experimental and refinement details of $Ca_2Ru_{1-x}Cr_xO_4$ with different x.

	$x=0$	$x=0.032$	$x=0.067$	$x=0.094$	$x=0.135$
Crystal data					
Chemical formula	$Ca_4Ru_2O_8$	$Ca_4Cr_{0.064}Ru_{1.936}O_8$	$Ca_4Cr_{0.134}Ru_{1.866}O_8$	$Ca_4Cr_{0.188}Ru_{1.812}O_8$	$Ca_4Cr_{0.27}Ru_{1.73}O_8$
M_r	490.46	474.02	474.02	474.02	469.85
Crystal system, space group	Orthorhombic, *Pbca*	Orthorhombic, *Pbca*	Orthorhombic, *Pbca*	Orthorhombic, *Pbca*	Orthorhombic, *Pbca*
Temperature (K)	90	90	90	90	90
a, b, c (Å)	5.3869 (2)[a], 5.6334 (2), 11.7349 (5)	5.3901 (1), 5.5909 (2), 11.7819 (4)	5.3917 (2), 5.5157 (2), 11.8804 (4)	5.3852 (2), 5.4454 (2), 11.9859 (4)	5.3160 (2), 5.2978 (3), 12.3091 (7)
V (Å^3)	356.11 (2)	355.05 (2)	353.31 (2)	351.48 (2)	346.66 (3)
Z	2	2	2	2	2
Radiation type	Mo $K\alpha$	Mo $K\alpha$	Mo $K\alpha$	Mo $K\alpha$	Mo $K\alpha$
μ (mm^{-1})	7.13	6.95	6.99	7.02	7.07
Crystal size (mm)	$0.08\times0.08\times0.04$	$0.08\times0.05\times0.04$	$0.05\times0.05\times0.05$	$0.10\times0.08\times0.05$	$0.08\times0.05\times0.04$
Data collection					
Diffractometer	Nonius KappaCCD diffractometer	Nonius KappaCCD diffractometer	Nonius KappaCCD diffractometer	Nonius KappaCCD diffractometer	Nonius KappaCCD diffractometer
Absorption correction	Multi-scan SADABS[b]	Multi-scan SADABS[b]	Multi-scan SADABS[b]	Multi-scan SADABS[b]	Multi-scan SADABS[b]
No. of measured, independent and observed[$I>2\sigma(I)$] reflections	6050, 399, 342	7175, 396, 367	7241, 398, 352	6955, 390, 362	7546, 441, 338
R_{int}	0.031	0.025	0.03	0.025	0.033
Refinement					
R[$F^2>2\sigma(F^2)$], $wR(F^2)$, S	0.021, 0.055, 1.11	0.016, 0.037, 1.10	0.016, 0.046, 1.13	0.018, 0.049, 1.17	0.026, 0.068, 1.33
No. of reflections	399	396	398	390	441
No. of parameters	34	36	36	35	34
No. of restraints	0	0	0	0	0
$\Delta\rho_{max}$, $\Delta\rho_{min}$ (e Å^{-3})	0.73, −0.85	0.55, −0.60	0.66, −0.60	0.61, −1.10	0.97, −0.95

[a] Note that errors of the last digit given in parentheses represent only statistical errors, not systematic errors which may for instance arise from correlations between parameters.
[b] Ref. [14].

Table 3
Structure refinement results of $Ca_2Ru_{1-x}Cr_xO_4$ with different x at 90 K. The position of Ru atom is always (0,0,0).

Space group	*Pbca*				
	$x=0$	$x=0.032$	$x=0.067$	$x=0.092$	$x=0.135$
a (Å)	5.3869(2)	5.3901(1)	5.3917(2)	5.3852(2)	5.3160(2)
b (Å)	5.6334(2)	5.5909(2)	5.5157(2)	5.4454(2)	5.2978(3)
c (Å)	11.7349(5)	11.7819(4)	11.8804(4)	11.9859(4)	12.3091(7)
V (Å^3)	356.11(2)	355.05(2)	353.31(2)	351.48(2)	346.66(3)
Ca x/a	0.00297(12)	0.00462(8)	−0.00732(8)	0.00928(7)	0.0088(2)
Ca y/b	0.05957(14)	0.0555(1)	0.04771(13)	0.04074(12)	0.0165(2)
Ca z/c	0.35246(6)	0.35218(5)	0.35145(5)	0.35057(6)	0.34826(13)
O1 x/a	0.1937(4)	0.1951(3)	0.0608(4)	0.1975(3)	0.1953(9)
O1 y/b	0.3011(4)	0.3012(3)	−0.0190(3)	0.3011(3)	0.3042(10)
O1 z/c	0.0280(2)	0.02672(15)	0.16479(16)	0.02214(12)	0.0118(3)
O2 x/a	−0.0701(6)	−0.0665(4)	−0.1967(3)	−0.0556(4)	−0.0296(9)
O2 y/b	−0.0217(4)	−0.0212(3)	0.3008(3)	−0.0166(3)	−0.0063(7)
O2 z/c	0.1644(2)	0.16470(15)	0.02456(15)	0.16488(14)	0.1650(4)
Ru–O1 (Å)	2.018(2)	2.0087(17)	1.9907(16)	1.9724(14)	1.922(5)
Ru–O1 (Å)	2.021(2)	2.0103(16)	1.9915(16)	1.9740(14)	1.929(5)
Ru–O2 (Å)	1.970(2)	1.9769(17)	1.9878(18)	2.0008(17)	2.038(5)
Ru–O–Ru (deg)	149.46(13)	150.11(10)	151.14(10)	152.00(9)	154.0(3)
Θ − O1(deg)	13.419(47)	12.872(33)	11.966(38)	10.925(28)	6.098(76)
Θ − O2(deg)	11.626(68)	11.010(51)	9.970(55)	8.993(48)	4.528(1 3 8)

If we plot the Cr concentration dependence of the lattice parameters of $Ca_2Ru_{1-x}Cr_xO_4$ (Fig. 4), we can clearly see the effect of Cr-doping leads to a trend opposite to that of cooling (Refer to Fig. 2). With increased Cr concentration, the c axis is enormously elongated, reflecting the elongation of RuO_6 octahedra by Cr doping. Alternatively, the flattening of RuO_6 octahedra with decreasing temperature is suppressed by Cr doping. The increased volume of the unit cell on cooling, which indicated an extremely large orthorhombic distortion, is also shown to be suppressed with increasing Cr doping.

The tilt, rotation and bond angle changes in the structure of $Ca_2Ru_{1-x}Cr_xO_4$ are also suppressed by Cr doping. Dramatic changes of the three distortion angles are shown in Fig. 5. We observe significant decrease in tilt angles with increasing Cr: With 3.2% Cr concentration, Θ − O2 angle goes down to 11.0(5)°, comparing with 11.63(7)° for pure sample. When x increases to 0.135 the Θ − O2 angle has decreased to 4.53(14)°. The similar decrease of Θ − O1 and increase of Ru–O–Ru angles also provide evidence that increasing Cr concentration can suppress structure distortion. The close association of this unusual suppression of

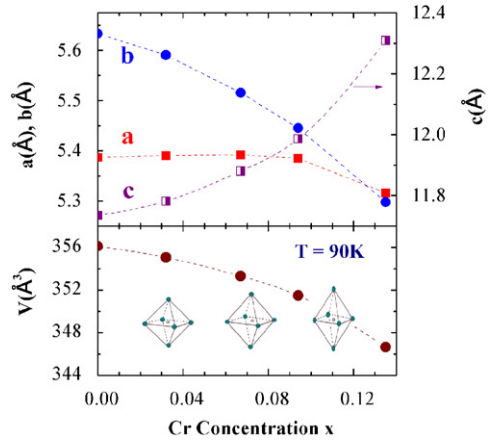

Fig. 4. Cr concentration dependence of the lattice parameters of $Ca_2Ru_{1-x}Cr_xO_4$, obtained from single-crystal X-ray diffraction.

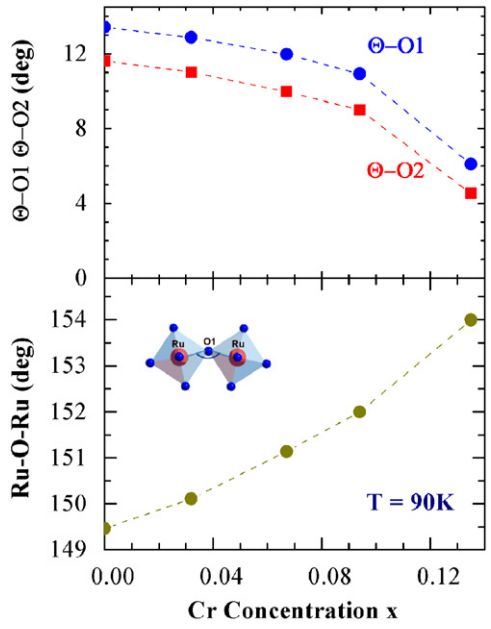

Fig. 5. Cr concentration dependence of the tilt, rotation and bond angles in $Ca_2Ru_{1-x}Cr_xO_4$, obtained from single-crystal X-ray diffraction. We use the same definition of $\Theta-O1$, $\Theta-O2$ and Ru–O–Ru distortion angles as in Fig. 3.

structural distortion with increasing Cr to different physical properties will be discussed in detail.

3.4. Transportation property and metal–insulator transition

Structural distortions discussed above are closely related to physical properties. The suppression of structural distortion with increasing Cr can be linked to colossal change of metal–insulator transition temperature (T_{MI}) in this system.

The resistivities as a function of temperature for different crystallographic directions are shown in Fig. 6. This abrupt transition from an insulating state to a nearly metallic state occurs at $T_{MI}=357$ K in pure compound [4]. In our $x=0.045$ sample, the sudden decrease by more than two orders of magnitude can be clearly observed and it characterizes a discontinuous alteration in the d-band structure typical of a metal–insulator transition [4]. Below the transition, $\rho(T)$ rises rapidly, increasing several orders of magnitude over a relatively narrow temperature interval. The wide hysteresis region in both *ab* plane and *c* axis are shown in Fig. 6,

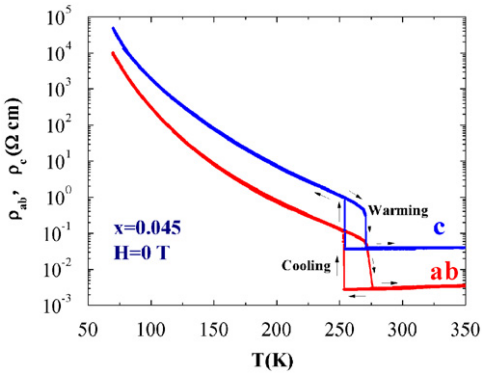

Fig. 6. Temperature dependence of electrical resistivity $\rho(T)$ when $I//ab$ and $I//c$ for $x=0.045$ sample.

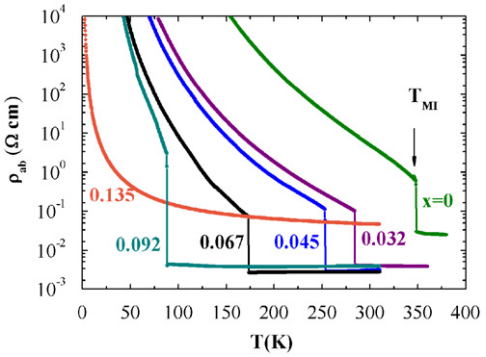

Fig. 7. Temperature dependence of in-plane electrical resistivity ρ_{ab} for $x=0$, 0.032, 0.045, 0.067, 0.092 and 0.135. This change of transition temperature also has been presented in Ref. [2].

indicating that the metal–insulator transition is first-order. T_{MI} happens at the same temperature on both *c* axis and *ab* plane, while the *c* axis has about one order larger resistivity throughout the temperature range. This structurally-driven metal–insulator transition can be related to the enhancement of structure distortion with decreasing temperature as discussed above. Structure distortion was enhanced at low temperature, leading to, an insulating phase.

In Fig. 7 the resistance is plotted on a logarithmic scale versus temperature. Upon Cr doping, the metal–insulator transition temperature (T_{MI}) decreases dramatically: For $x=0$, the metal–insulator transition occurs at $T_{MI}=357$ K and when $x=0.032$ T_{MI} drops to 284 K. With further Cr doping, T_{MI} decreases further, such that for $x=0.092$ the metallic phase is retained down to $T=81$ K. This continuous decrease of T_{MI} with the increasing Cr doping is directly related to the suppression of the structural distortion discussed above. The bandwidth W in this system depends critically on the Ru–O–Ru bond angle distortion. If we suppose there is a critical distortion angle where the metal–insulator (MI) transition happens, Cr doping suppresses the distortion in the system while cooling increases this distortion. Thus, increased Cr doping requires lower temperature to achieve this critical angle, which means the MI transition happens at lower temperature. The colossal change of T_{MI} can be interpreted as a competition between these two phenomena. These two effects rigorously compete, but Cr doping prevails eventually, thus, the overall disappearance of T_{MI} when Cr is higher than 13.5% can be seen in Fig. 7 [2]. After T_{MI} is suppressed, the system shows insulating behavior at low temperature, which means the energy gap is still open. Compared to other dopants such as La [6,22] or Sr [23,24], the impact of Cr doping on $\rho(T)$ is profoundly different: Cr substitutes on Ru site while La and Sr both occupy a Ca site. High concentrations of La or Sr make the system metallic, but

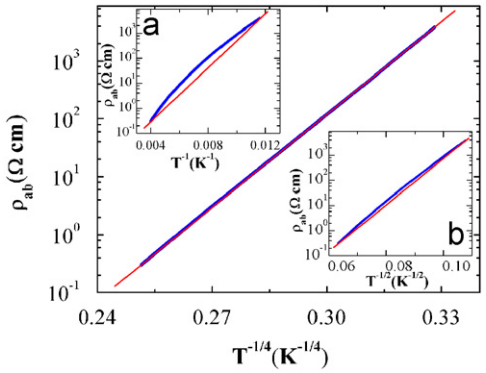

Fig. 8. Fit of the electrical resistivity in the *ab* plane, $\rho(T)$, of single crystal $Ca_2Ru_{1-x}Cr_xO_4$ for $x=0.032$ to variable-range hopping with $n=3$. Inset: (a) Fit to activation-type insulating behavior were not good; and (b) variable-range hopping with $n=1$ is less good.

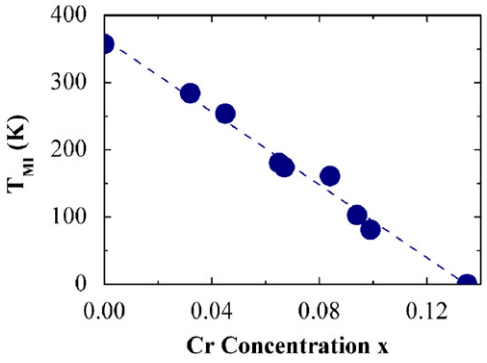

Fig. 9. Cr concentration dependence of T_{MI} (metal–insulator transition temperature).

rich Cr doping makes the system an insulator at low temperature due to suppression of the metal–insulator transition.

The amplitude of $\rho(T)$ for doped sample decreases more than one order of magnitude throughout the entire measured temperature range compared to pure sample. For all samples with $0<x<0.10$, a metallic phase at $T>T_{MI}$ can be well established. In order to elucidate the electronic state in the insulating phase, we analyze the electrical resistivity in the *ab* plane, ρ_{ab}, of single crystal $Ca_2Ru_{1-x}Cr_xO_4$ for $x=0.032$. As shown in Fig. 8, the result does not fit well to activation-type insulating behavior [23]: $\rho(T)=A\exp(E_G/2k_BT)$ in the temperature range $70<T<300$ K. In the same T region of insulating phase, $\rho(T)$ can well fit to the Efros–Shklovskii mechanism. The Efros–Shklovskii mechanism can be given by $\rho(T)=A\exp(T_0/T)^{1/(n+1)}$ ($n=1$, 2, 3), which represents the n dimensional variable-range hopping (VRH) without interaction among the localized electrons: T_0 is the characteristic temperature. In almost all concentrations of Cr, VRH fits of $\rho(T)$ were much better than the activation law. However, the behavior of the low temperature $\rho(T)$ for pure sample and Cr doped sample is fundamentally different. For pure sample ($x=0$), VRH fits best with $n=1$ [1,4]. While for $x>0$, VRH fits best when $n=3$, as shown in Fig. 8, thus Cr doping fundamentally changes the low temperature range conductivity behavior.

4. Conclusions

$Ca_2Ru_{1-x}Cr_xO_4$ single crystals with different Cr concentrations were synthesized by the floating zone method and studied by high resolution single crystal X-ray diffraction. The change of lattice parameters and distortions in the structure were studied in detail. We found the RuO_6 octahedrons are flattened with decreasing T, and structure distortion is enhanced at low temperature. Cr-doping leads to an opposite trend. Strong suppression of structure distortion was found in Cr rich samples. The competition of Cr doping and cooling results in a colossal change of metal–insulator transition temperature. We observe a suppression of T_{MI} when $x>13.5\%$, indicating that the effect of Cr doping prevails eventually. In the plot of Cr concentration dependence of T_{MI} (Fig. 9), we can clearly see this decrease of T_{MI} with increasing Cr concentration. The dashed line in Fig. 9 separated the insulating region on bottom and conducting region at the top.

Ca_2RuO_4 is a rare model system for investigating questions of metal–insulator transitions because of its unusual ground-state instability, and the interplay of charge, spin, and orbital degrees of freedom. Cr doping can effectively suppress the structure distortion, and provides a good opportunity to study the metal–insulator transition in this system. Such a large and sharp metal–insulator transition, with a transition temperature that is tuneable by virtue of dopant concentration, may have potential applications in electronic devices.

Acknowledgments

We are thankful to Dr. J.W. Brill for useful discussions. This work was supported by NSF grants DMR-0552267, DMR-0856234 and EPS-0814194.

References

[1] G. Cao, S. McCall, M. Shepard, J.E. Crow, R.P. Guertin, Phys. Rev. B 56 (1997) R2916–R2919.
[2] T.F. Qi, O.B. Korneta, S. Parkin, L.E. De Long, P. Schlottmann, G. Cao, Phys. Rev. Lett. 105 (2010) 177203.
[3] M.A. Carpenter, C.J. Howard, Acta Crystallogr. B 65 (2009) 134–146.
[4] C.S. Alexander, G. Cao, V. Dobrosavljevic, S. McCall, J.E. Crow, E. Lochner, R.P. Guertin, Phys. Rev. B 60 (1999) R8422–R8425.
[5] A.V. Puchkov, M.C. Schabel, D.N. Basov, T. Startseva, G. Cao, T. Timusk, Z.X. Shen, Phys. Rev. Lett. 81 (1998) 2747–2750.
[6] G. Cao, S. McCall, V. Dobrosavljevic, C.S. Alexander, J.E. Crow, R.P. Guertin, Phys. Rev. B 61 (2000) R5053–R5057.
[7] I. Zegkinoglou, J. Strempfer, C.S. Nelson, J.P. Hill, J. Chakhalian, C. Bernhard, J.C. Lang, G. Srajer, H. Fukazawa, S. Nakatsuji, Y. Maeno, B. Keimer, Phys. Rev. Lett. 95 (2005) 136401.
[8] M. Braden, G. Andre, S. Nakatsuji, Y. Maeno, Phys. Rev. B 58 (1998) 847–861.
[9] O. Friedt, M. Braden, G. Andre, P. Adelmann, S. Nakatsuji, Y. Maeno, Phys. Rev. B 6317 (2001) 174432.
[10] P. Steffens, O. Friedt, P. Alireza, W.G. Marshall, W. Schmidt, F. Nakamura, S. Nakatsuji, Y. Maeno, R. Lengsdorf, M.M. Abd-Elmeguid, M. Braden, Phys. Rev. B 72 (2005) 094104.
[11] G. Cao, V. Durairaj, S. Chikara, L.E. DeLong, P. Schlottmann, Phys. Rev. Lett. 100 (2008) 016604.
[12] M. Imada, Phys. Rev. B 72 (2005) 075113.
[13] G.M. Sheldrick, Acta Crystallogr. A 64 (2008) 112–122.
[14] G.M. Sheldrick, SADABS, University of Gottingen, Germany, 1996.
[15] S. Parkin, B. Moezzi, H. Hope, J. Appl. Crystallogr. 28 (1995) 53–56.
[16] V.Z. Pletnev, V.T. Ivanov, D.A. Langs, B.M. Burkhart, W.L. Duax, Biopolymers 42 (1997) 645–650.
[17] K. Brandenburg, Diamond, version 3.1 Crystal Impact GbR, Bonn, Germany (2007).
[18] R. Shaheen, M.J. Akhtar, M. Nadeem, M.N. Haque, J. Phys. Chem. Solids 64 (2003) 237–245.
[19] J.M. Chen, T.L. Chou, J.M. Lee, S.A. Chen, T.S. Chan, T.H. Chen, K.T. Lu, W.T. Chuang, H.S. Sheu, S.W. Chen, C.M. Lin, N. Hiraoka, H. Ishii, K.D. Tsuei, T.J. Yang, Phys. Rev. B 79 (2009) 165110.
[20] A. Niazi, S.L. Bud'ko, D.L. Schlagel, J.Q. Yan, T.A. Lograsso, A. Kreyssig, S. Das, S. Nandi, A.I. Goldman, A. Honecker, R.W. McCallum, M. Reehuis, O. Pieper, B. Lake, D.C. Johnston, Phys. Rev. B 79 (2009) 104432.
[21] M.A. Carpenter, C.J. Howard, Acta Crystallogr. B 65 (2009) 147–159.
[22] H. Fukazawa, Y. Maeno, J. Phys. Soc. Jpn. 70 (2001) 460–467.
[23] S. Nakatsuji, V. Dobrosavljevic, D. Tanaskovic, M. Minakata, H. Fukazawa, Y. Maeno, Phys. Rev. Lett. 93 (2004) 146401.
[24] M. Kriener, P. Steffens, J. Baier, O. Schumann, T. Zabel, T. Lorenz, O. Friedt, R. Muller, A. Gukasov, P.G. Radaelli, P. Reutler, A. Revcolevschi, S. Nakatsuji, Y. Maeno, M. Braden, Phys. Rev. Lett. 95 (2005) 267403.